Comparison of energetic spanwise modes in a boundary layer and channel

by

Christopher D. Tomkins and Ronald J. Adrian

University of Illinois at Urbana-Champaign
Department of Theoretical and Applied Mechanics
Urbana, IL 61801

ABSTRACT

The spanwise organization and energy contribution of motions in a $Re_\theta = 1015$ flat-plate turbulent boundary layer are investigated using PIV in the streamwise-spanwise plane. Measurements are performed at several heights: $y^+ = 21$, 46, and 92 ($y/\delta = 0.05$, 0.11, and 0.22). Dual cameras mounted side-by-side obtain a wide field of view in the spanwise direction, capturing nearly 1100 viscous units (2.55δ). Two-dimensional Fourier analysis is used to estimate the energy distribution of the streamwise component as a function of distance from the wall. The results ($Re_t = u_t d/n = 426$, based on boundary layer thickness) are compared with the channel flow data of Liu *et al.* (2000) ($Re_t = u_t h/n = 400$, where h is channel half-height) at a comparable wall-normal location.

Liu *et al*. showed the well-established streak spacing mode of $\lambda_z^+ = 100$ contains surprisingly little energy relative to modes in the range $\lambda_z^+ = 200\text{-}400$. A principal objective of the present work is to determine if this result is universal for wall-bounded flows. The boundary layer results show strong agreement with the channel in terms of the spanwise energy contribution of the small scales near the wall: over 75% of the energy is in scales larger than $\lambda_z^+ = 100$. The spanwise energy distribution of the smaller streamwise scales also shows excellent agreement. However, differences in the spanwise energy distribution between the boundary layer and channel flow appear in the large streamwise modes. As a result, the spanwise energy distribution at $y^+ \approx 21$ is not universal for all scales.

1. INTRODUCTION

It is well known that low and high-speed streaks exist in the near-wall region of turbulent wall flows. Previous investigations have typically used flow visualization to investigate streak spacing and characteristics, including the seminal work of Kline *et al*. (1967) who identified the mean spanwise spacing of $l^+_z = 100$, and Smith and Metzler (1983) who showed the spacing has a lognormal distribution and increases with distance from the wall. In these and numerous other studies the spanwise streak spacing of $l^+_z = 100$ is universally accepted, and generally considered one of the successes of turbulence structure research.

Several investigations have studied the spanwise organization and properties of motions further from the wall. Wark and Nagib (1991) investigated a $Re_\theta = \theta U_\infty/\nu = 4650$ boundary layer using conditional averaging and observed "roller-type" structures extending several δ streamwise and approximately 0.5 δ spanwise. These motions were associated with Reynolds stress production, and sweeps and ejections were observed to occur in a "quasi-periodic" manner spanwise, even in the larger scales. Tomkins and Adrian (1999) performed wide-view PIV measurements in the streamwise-spanwise plane of a boundary layer at $Re_\theta = 7705$. Horizontal planes of data at $y/\delta = 0.2$ revealed large-scale regions of *u*-momentum deficit highly elongated in the streamwise direction bordered by sequences of concentrated vertical vorticity. Regions of high speed fluid, also elongated streamwise, were typically observed occupying the gaps between neighboring areas of momentum deficit. The observations are consistent with the *x-y* plane results of Adrian *et al*. (2000), among others, and the *x* and *z* characteristics of the large-scale motions are consistent with those in Wark and Nagib (1991).

Scaling of two-point correlation functions with spanwise separation is quite well documented. McLean (1980) performed two-point correlations of streamwise velocity as a function of wall-normal distance over a significant range of Reynolds numbers ($1500 < Re_\theta < 10290$). The author found $R_{uu}(z)$ scales with outer variables throughout the boundary layer except for small separations in the region $y^+ < 40$. Wark *et al*. (1991) investigated behavior of the correlation function $R_{\tau u}(z)$, where τ is the streamwise wall shear stress, over the Reynolds number range $670 < Re_\theta < 5961$. The correlation was found to scale with outer units for all displacements and wall-normal locations, with the exception of displacements less than $z^+ = 40$ very near the wall ($y^+ \approx 10\text{-}15$).

The present investigation is motivated in large part by recent results (Liu *et al*., 2000) in a $Re_t = u_t h/n = 400$ (*h* is channel half-height) turbulent channel flow. Measurements reveal that while the established $l^+_z = 100$ mode is energetic, much larger spanwise modes actually contribute more to the streamwise turbulent kinetic energy, even at $y^+ = 20$. While it is not surprising that the peak energy is greater than identically $l^+_z = 100$ (e.g. Kline *et al*., 1967 found peak energy $l^+_z \approx 130$), the scale of the energetic modes is surprising, with significant energy in the range $l^+_z = 200\text{-}400$. The result has implications regarding the influence of large-scale motions in the near-wall region, but it has yet to be observed in another experiment or apparatus.

The aim of the present work is to investigate spacing, growth, and energy contribution of structures as a function of distance from the wall in a zero pressure gradient flat-plate turbulent boundary layer at $Re_\theta = 1015$. Particle image velocimetry (Adrian, 1991) measurements are made in the streamwise-spanwise plane at several wall-normal locations ($y^+ = 21$, 46, and 92; $y/\delta = 0.05$, 0.11, and 0.22). The measurements have a wide field of view spanwise (2.55δ) to capture a wide range of modes, and a large number of samples (200) for good statistical convergence. The $Re_\theta = 1015$ flow offers a similar $Re_t = u_t d/n$ as the Liu *et al*. (2000) channel flow, $Re_t = 426$. One principle objective of the present work is to determine if the near-wall low Reynolds number channel flow results of Liu *et al*. (2000) can be replicated at a similar height ($y^+ = 21$) in a boundary layer of comparable Reynolds number. This is the focus of the present paper. The issue has implications on the universality of the near-wall region in wall-bounded flows.

2. EXPERIMENT

2.1 Flow Facility and Parameters

Measurements are performed in a low-turbulence open circuit Eiffel-type wind tunnel. Flow is drawn in through a series of screens and honeycombs and accelerated into the test section, in which the free-stream turbulence intensity is estimated to be 0.16%. The boundary layer develops over a smooth, flat plate with dimensions 6096 mm streamwise (x) by 914 mm spanwise (z); this width is greater than ten times the boundary-layer thickness so side effects are minimal. Zero pressure gradient is obtained by adjusting the height of the roof in the test section. The layer is tripped with a 4.7 mm diameter rod laid flat along the plate at $x = 1520$ mm. The center of the measurement volume is located at $x = 5310$ mm from the leading edge. A thorough description of the facility is given in Meinhart (1994).

A Reynolds number $Re_\theta = \theta U_\infty/\nu = 1015$ boundary layer is considered, where θ is the momentum thickness, U_∞ the free stream velocity, and ν the air kinematic viscosity. The experiment is designed to closely match one set of x-y plane measurements in Adrian *et al.* (2000) by matching all controllable parameters. Errors in Reynolds number between the two experiments due to differences in atmospheric pressure are within 2%. Table 1 shows several relevant flow parameters calculated from the x-y measurements. The momentum thickness is calculated by numerically integrating the boundary-layer profile, the wall friction velocity u_τ is estimated using the Clauser (1956) chart method, and the boundary layer thickness δ is calculated using the 0.99 criterion.

2.2 Measurement Details

Two-dimensional velocity measurements are obtained in horizontal planes at several y-locations using digital PIV. Relevant measurement parameters are summarized in Table 2. The measurement heights are chosen to extend from the near-wall region to the top of the logarithmic layer. The low Reynolds number measurement height nearest the wall corresponds with the channel flow data of Liu *et al.* (2000) in terms of viscous wall units ($y^+ = 21$); this data set is the focus of the current paper.

The experiments are designed to capture a wide field of view, particularly in the spanwise direction, which extends 1085 viscous wall units at the low Reynolds number. Images are captured using two 2k by 2k CCD cameras set side-by-side, giving a 2:1 spanwise-streamwise view aspect ratio with a 4k by 2k pixel array. The images are registered mechanically using a calibration target and micro-adjustments to camera position. Camera alignment is to within 1 pixel out of 2000 vertically, horizontally, and with respect to rotation. Images are combined before interrogation. An enlarging lens, specially designed to minimize distortion, is placed backwards in this system to eliminate wide-view distortions. Olive-oil particles of nominal 1-2 micron diameter are illuminated using two Nd:YAG pulsed lasers which produce approximately 150 mJ per pulse @ 532 nm. The laser beam is spread using negative cylindrical lenses into a sheet of 130 mm in the test section, crossing the flow in the spanwise direction. The sheet is focused using a positive spherical lens to a waist near the middle of the test section; its greatest thickness in the field of view is roughly 0.5 mm. The sheet is aligned parallel to the boundary layer plate using alignment blocks with thin grooves precisely machined in at specified heights. Light is scattered from particles through a float glass plate in the test section floor to a 45 degree angled mirror underneath the tunnel, and collected by the lenses described above. The timing of the lasers and cameras was controlled by a TSI, Inc. synchronizer box. Time between pulses was set at 100 μs resulting in average particle image displacements in the range 11-15 pixels.

TABLE 1: FLOW PARAMETERS

Re_θ ($U_\infty\theta/\nu$)	U_∞ (m/s)	θ (mm)	u_τ (m/s)	y^* (mm)	δ (mm)	$Re_t = \delta^+$	Resolution, z^+	Resolution, x^+
1015	1.77	8.84	0.086	0.179	76.2	426	5.6	7.0

TABLE 2: MEASUREMENT PARAMETERS

Re_θ	y^+	y/δ	Streamwise field of view (x/δ)	Streamwise field of view (x^+)	Spanwise field of view (z/δ)	Spanwise field of view (z^+)	Number of Realizations
1015	21	0.05	1.08	460	2.55	1085	201
1015	46	0.11	1.08	460	2.55	1085	201
1015	92	0.22	1.08	460	2.55	1085	201

2.3 Interrogation

The double-exposed images are interrogated using single frame cross-correlation with a discrete window offset specified *a priori*. The interrogation is carried out using PIV Sleuth software (Christensen *et al*., 2000). No image shifting is necessary at these locations in this zero-pressure gradient layer; the velocities never approach zero. Slightly rectangular spot sizes are used for the first window to improve resolution in the spanwise direction, 36 pixels spanwise by 44 pixels streamwise. The second window is set at 64 by 64 pixels, and the first window is zero-padded to this size for correlation via FFTs. Window offset is chosen to place the correlation peak near the center of the correlation plane and hence remove any bias due to edge effects. The particle image diameter d_τ was on average 3 pixel diameters, giving d_τ/d_{pix} sufficiently large to minimize bias errors due to image discretization (Adrian, 1995; Westerweel, 1997). Peak fitting is done using a Gaussian 3-point estimator. The measurement volume in the fluid is defined by the interrogation spot size in x and z and the light sheet thickness in y. In terms of viscous wall units the measurement volume is $\Delta x^+ = 14$, $\Delta z^+ = 11$, and $\Delta y^+ = 2.8$. 50% overlap of interrogation spots yields measurement resolution of $7x^*$ by $5.6z^*$. This may not resolve all of the scales of the turbulence. However, the measurements resolve the structures of interest while simultaneously capturing very large scales. The above procedure yields approximately 20,000 vectors with a low percentage of obviously spurious measurements. The raw fields are validated by systematic removal of bad vectors and replacement with 2nd and 3rd choices in the correlation plane where appropriate. One pass of interpolation given a high percentage of neighboring valid measurements is performed, and finally a narrow Gaussian filter is applied to remove noise.

3. RESULTS

Statistical quantities in the current measurements are calculated by ensemble averaging over all realizations and then averaging over both homogeneous directions in the ensemble average. Figure 1 shows mean streamwise velocity at each height plotted in outer units against the mean velocity profile measured in Adrian *et al*. (2000). Good agreement is found between the data sets. In Figure 2 fluctuating streamwise velocity is plotted against the *x-y* data; again agreement is good. The *x-z* plane data points are consistently slightly below the *x-y* plane curve. This difference may be a manifestation of the limited resolution of the data, although the points are within the sampling error of the *x-y* plane measurements for 2nd order statistics.

The quantitative nature of the PIV measurements allows for high-resolution statistical analysis. However, vector or contour plots of instantaneous fields may also be used for flow visualization. Counting the number of low speed streaks visually allows for comparison of streak spacing with previous studies. The procedure followed here is identical to that in Liu *et al*. (2000), i.e. the mean streak spacing is taken to be the reciprocal of the average number of streaks per unit width over all realizations at a given height. The results of this procedure are plotted in Figure 3 as a function of wall-normal location, along with the results from Liu *et al*. (shown in grey), and a set of results from other researchers collected by Kasagi (1988). The present results are clearly consistent with the relatively wide range of data previously observed. As expected, the streak spacing starts around $I^+_z = 100$ very near the wall and increases with y. At $y^+ = 21$, mean spacing is approximately $I^+_z = 120$.
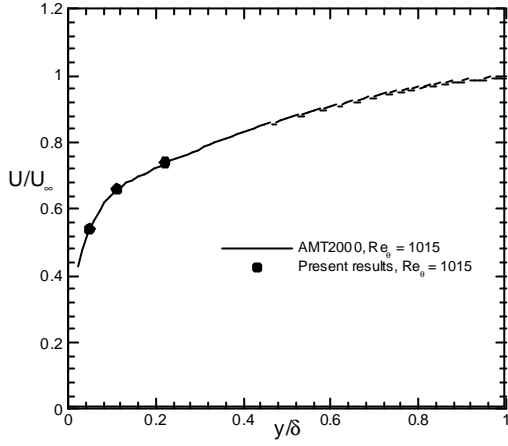
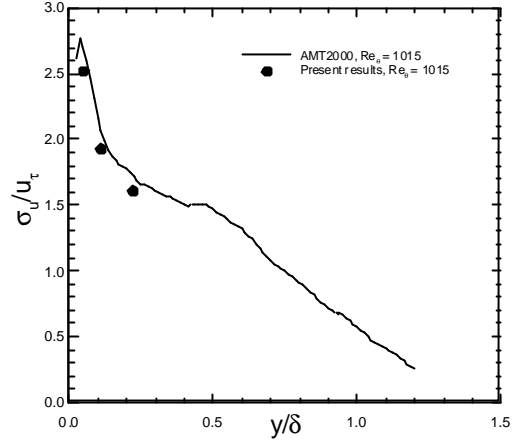Figure 1. Mean streamwise velocity at 3 measurement heights. Comparison with results in Adrian et al., 2000.

Figure 2. RMS streamwise velocity at 3 measurement heights. Comparison with results in Adrian et al., 2000.

3.1 Fourier Analysis of the Velocity Field

Flow visualization of the instantaneous fields provides an estimate of streak spacing. The planar PIV data, however, allows for more highly resolved quantitative analysis. Two-dimensional power spectra of the streamwise velocity are calculated in horizontal planes as a function of distance from the wall at both Reynolds numbers. The spectra reveal the distribution of turbulent kinetic energy among streamwise and spanwise modes.

The two-dimensional spectral density function of the fluctuating velocity is given by the Fourier transform of the normalized two-point spatial correlation function $R_{ij}(r_x, y, r_z)$,

$$\boldsymbol{f}_{ij}(k_x, y, k_z) = \iint R_{ij}(r_x, y, r_z) e^{-j(k_x \cdot r_x + k_z \cdot r_z)} dr_x dr_z$$

where k_x and k_z are the streamwise and spanwise wavenumbers, respectively. The wavenumber k is related to the wavelength λ by $k = 2\pi/\lambda$. The subscripts i and j denote the streamwise or spanwise directions. For discrete data, the two-point spatial correlation coefficient is estimated as:

$$R_{ij}(r_x, y, r_z) = \frac{\displaystyle\sum_x \sum_z u_i(x, y, z) u_j(x + r_x, y, z + r_z)}{\sqrt{\displaystyle\sum_x \sum_z u_i^2(x, y, z)} \sqrt{\displaystyle\sum_x \sum_z u_j^2(x + r_x, y, z + r_z)}}$$

where the summations are carried out over each x and z in every realization, and r_x and r_z represent the separations of the two points in the homogeneous streamwise and spanwise directions, respectively. The wavenumbers are nondimensionalized using $k^+ = 2\pi/\lambda^+ = 2\pi y^*/\lambda$, and the spectra normalized with total energy.

3.2 Comparison of Power Spectra

Liu $et\ al.$ (2000) computed two-dimensional spectra in their $Re_t = u_t h/\boldsymbol{n} = 400$ turbulent channel flow at $y^+ = 20$. As discussed in the introduction, the spectra reveal energy in the streamwise component is distri-

λ$_z^+$

700
600
500
400
300
200
100

Smith & Metzler
Rajaee et al.
Iritani et al.
Liu et al.
Kline & Schraub
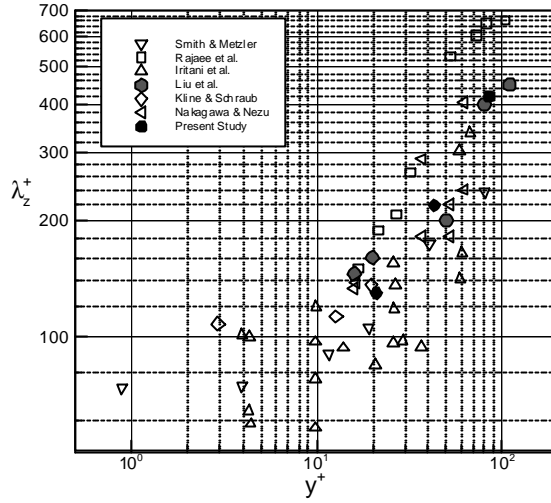Nakagawa & Nezu
Present Study

10^0 10^1 10^2

y^+

Figure 3. Estimation of low speed streak spacing by visual counting as a function of wall-normal location. Comparison with results of Liu et al., 2000 (gray symbols) and several studies compiled by Kasagi (1988).

buted in much larger spanwise scales than the expected $I^+_z = 100$ determined from streak counting in flow visualization. In the present work, measurements are performed in the $Re_\theta = 1015$ boundary layer at $y^+ = 21$ for comparison. In this flow $Re_t = u_t d/n = 426$, comparable to the Liu *et al.* flow, though here δ is chosen as the outer length scale. Whether or not the outer scales of the flow influence the near-wall energy distribution is an issue of interest. An informative way of viewing the two-dimensional spectra is to extract several "slices" of data corresponding to specific streamwise wavenumbers, and observe how the energy in these particular *streamwise* modes varies as a function of *spanwise* wavenumber.

This is done in Figure 4, which contains data for both the Liu *et al.* channel flow (hollow symbols) and the low Reynolds number boundary layer (solid symbols). Here premultiplied power spectra of the streamwise component $k^+_z \Phi^+_{uu}(k^+_x, y, k^+_z)$ is plotted versus spanwise wavenumber k^+_z, for several values of the streamwise wavelength, I^+_x. The values of I^+_x are chosen to correspond with the values in Liu *et al.*, and several values of the spanwise wavenumber k^+_z are marked on the abscissa. The agreement between the data sets is quite good considering they represent different flows measured in different facilities. In both flows, $I^+_z = 100$ is an energetic mode, but much more energy is contained in larger scales, in the range $I^+_z = 150$-400. As discussed in Liu *et al.*, this is significantly higher than one would expect based on flow visualization measurements. So with regards to this observation, the channel and boundary layer are in good agreement. The trend of increasing energy with decreasing streamwise wavenumber is also apparent in Figure 3, as the largest streamwise modes clearly contain the most energy. Furthermore, that energy is contained in increasingly large spanwise modes as streamwise wavelength increases. Hence, the larger spanwise modes are more energetic even when integrating over all streamwise wavenumbers.

Examining the spanwise energy distribution in individual streamwise modes is informative. Consider the streamwise modes in the range $I^+_x = 400$-470, plotted with green "del" symbols. These modes represent the moderately high wavenumber, inner-layer scales. Peak energy is in the range $I^+_z = 120$-150, quite close to the observed streak spacing of approximately $I^+_z = 120$ at this height. This is consistent with the idea that the shorter streamwise modes represent the near-wall structures, and subsequently reflect the streak spacing more closely. Furthermore, these modes are in close agreement for both facilities, suggesting the near-wall structures maintain a universal behavior in wall turbulence.
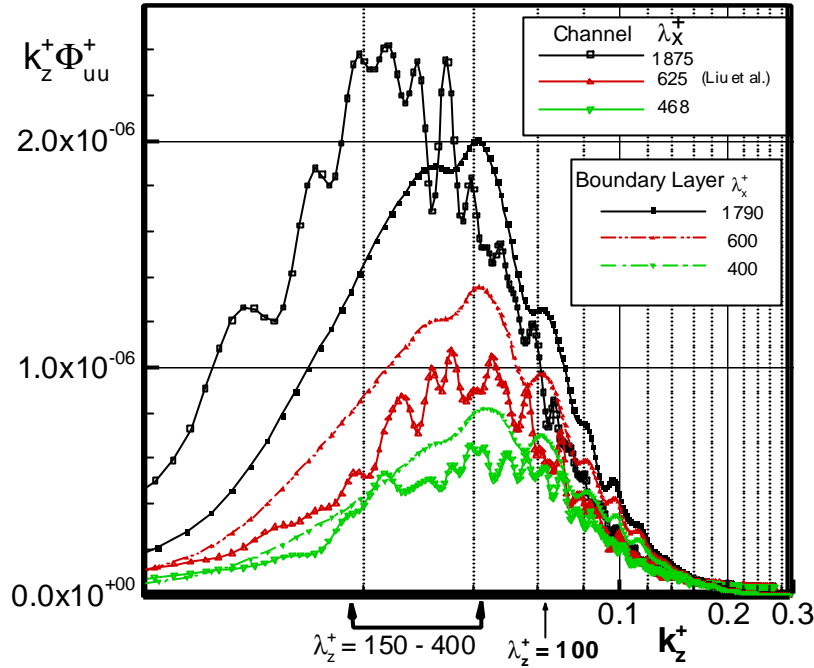
Figure 4. Premultiplied power spectra of the streamwise component versus spanwise wavenumber for several values of the streamwise wavelength. Comparison with the channel flow results of Liu et al.(2000).

There is a difference between the boundary layer and channel, however, in the distribution of energy in the largest streamwise wavelength, plotted with squares. These highly energetic streamwise modes represent the largest scales, presumably the scales of the outer region. It is in the modes representing these motions that the differences in the facility and flow are manifest (and it has already been seen that these modes dominate the energy, even near the wall). In Figure 4, it may be seen that differences in the spanwise energy distribution of the large streamwise motions persist right down to $y^+ = 21$. In summary, universality is observed in the spanwise energy distribution of the near-wall motions, represented by the higher streamwise wavenumber modes. However, the outer scales influence the energy distribution of the lower streamwise wavenumber modes, which dominate the turbulent kinetic energy even close to the wall, preventing universal behavior over all scales.

The cumulative spectral energy contained within all spanwise modes up to some l^+_z is obtained by integration of the spectra over all streamwise modes to obtain one-dimensional spectra in k^+_z, and then integration from $k^+_{z,maximum}$ down to some k^+_z. This gives a quantitative estimate of the contribution to the total streamwise energy from various bands of spanwise modes. Cumulative energy is plotted in Figure 5 for the boundary layer and channel at similar height. The percentage of energy contained in spanwise modes less than l^+_z, normalized by the total energy, is plotted against l^+_z. The boundary layer is again represented by solid symbols, and the channel flow hollow symbols. The agreement between the two data sets is excellent for the smaller scales, so the principle conclusion of Liu *et al.* for the channel is found to be true for the boundary layer: near the wall ($y^+ = 21$), a significant fraction of energy, greater than 75%, is contained in modes much larger than $l^+_z = 100$. As spanwise scale increases the difference between the curves increases, becoming significant for the large scales. This may again be a manifestation of the differences in the large scales imposed by the different conditions in the flow facilities. There may also be a slight Reynolds number effect. The $Re_t = 426$ in the boundary layer is based on δ, while the $Re_t = 400$ in the channel is based on half-height h. δ is certainly an appropriate scale of the outer edge of the boundary layer, but structures in channel flow are observed extending beyond the half-height, to approximately 60-70% of $2h$. Thus, one could very roughly define an equivalent δ for the channel, say, $\delta_{ch} = 7/5\ h$, representing the outer edge of the flow from one wall. This would result in an equivalent $Re_t = u_t \delta_{ch}/\nu$ of
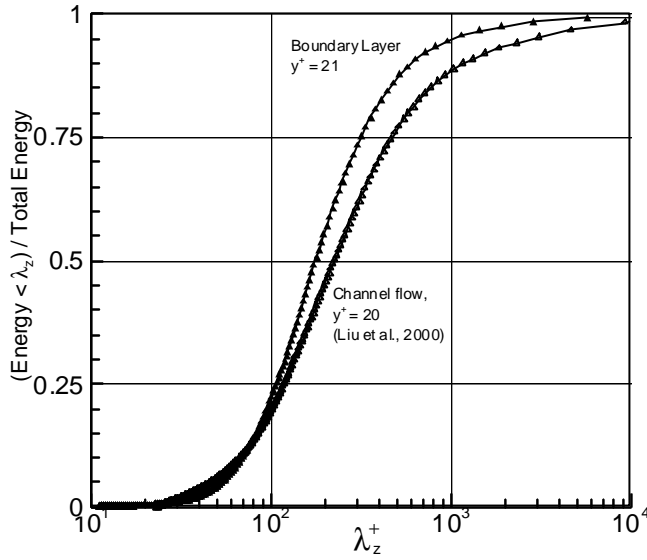
Figure 5. Normalized cumulative spectral energy versus spanwise wavelength. Comparison with Liu et al. (2000) channel flow.

560, representing an approximate increase in Reynolds number of 25%. The results of McLean (1980) indicate scaling of spanwise correlations in the near-wall region is a function of the separation variable. For shorter separations inner scaling is appropriate, and indeed the two curves in Figure 4 collapse for smaller streamwise motions when plotted with inner variables, as do the curves in Figure 5 for smaller spanwise wavelengths. For larger motions, correlations were found to scale with outer variables even near the wall. This is consistent with the shift towards smaller k^+_z in the channel flow for the largest l^+_x curve in Figure 4, and consistent with the shift towards larger scales in the region of large l^+_z in Figure 5. However, this Reynolds number effect does not fully reconcile the discrepancies between the curves. Hence, one must conclude the discrepancies are likely a manifestation of the fundamental differences between the boundary layer and channel.

CONCLUSIONS

The organization and energy contribution of motions in a flat-plate turbulent boundary layer are investigated experimentally using PIV in the streamwise-spanwise plane at $Re_\theta = 1015$. 201 realizations are captured at each of several heights: $y^+ = 21$, 46, and 92 ($y/\delta = 0.05$, 0.11, and 0.22). Dual cameras mounted side-by-side are used to obtain a wide field of view in the spanwise direction, capturing nearly 1100 viscous units (2.55δ). Two-dimensional Fourier analysis is employed to estimate the energy distribution of the streamwise component as a function of distance from the wall. Integration in both k_x and k_z yields cumulative energy within a specified range of modes. The large number of samples allows for good statistical convergence.

The data provides strong complementary evidence to the $Re_\tau \approx 400$ channel flow results of Liu *et al.* (2000), who showed the well-established spanwise streak spacing mode $\lambda_z^+ = 100$ contains relatively little turbulent kinetic energy even near the wall ($y^+ = 20$), while modes in the range $\lambda_z^+ = 200\text{-}400$ were dominant in terms of energy. The present low Reynolds number boundary-layer results ($Re_\theta = 1015$, $Re_\tau \approx 425$) at an equivalent wall-normal location ($y^+ = 21$) show strong agreement with the channel flow results in terms of the energy contribution of the smaller spanwise scales: over 75% of the energy is in scales larger than $\lambda_z^+ = 100$. In addition, the spanwise energy distribution of the smaller streamwise scales shows

excellent agreement. These complimentary experiments measure different flows in separate facilities and are obtained with independent diagnostic systems, suggesting these results are both reliable and universal.

Differences in the energy distribution between the boundary layer and channel flow appear in the large streamwise and spanwise modes. These modes represent the outer scales of the flow, and are influenced by boundary conditions in the flow facility; it is through these modes that the differences in the two flows are evident. It is also shown the large-scale modes dominate the turbulent kinetic energy even near the wall in the boundary layer and channel. As a result, the spanwise energy distribution at $y^+ \approx 21$ is not universal over all scales.

REFERENCES

Adrian, R. J., 1991, Particle-imaging techniques for experimental fluid mechanics, *Ann. Rev. Fluid Mech.*, vol. 23, pp.261-304.

Adrian, R. J., 1995, Limiting resolution of particle image velocimetry for turbulent flow, *Advances in Turbulence Research*, pp. 1-19, Postech, Pohang, Korea.

Adrian, R. J., Meinhart, C. D., and Tomkins, C. D., 2000, Vortex organization in the outer region of the turbulent boundary layer, *J. Fluid Mech.*, in press.

Christensen, K. T., Soloff, S. M. & Adrian, R. J. 2000. PIV Sleuth: Integrated Particle Image Velocimetry (PIV) Interrogation/Validation Software. *TAM Report* No. 943, University of Illinois.

Clauser, F., 1956, The turbulent boundary layer, *Advances in Applied Mechanics*, vol. 4, pp.1-51.

Kasagi, N., 1988, Structural study of near-wall turbulence and its heat transfer mechanism, *Near-wall Turbulence*, Zoran Zaric Memorial Conference, pp. 596-619.

Kline, S. J., Reynolds, W. C., Schraub, F. A., and Runstadler, P. W., 1967, The structure of turbulent boundary layers, *J. Fluid Mech.*, vol. 30, part 4, pp. 741-773.

Liu, Z.-C., Adrian, R. J., and Hanratty, T. J., 2000, Spanwise modes of streaky structures in a turbulent channel flow, in preparation.

McLean, I. R., 1980, The near wall eddy structure in an equilibrium turbulent boundary layer, Ph.D. Thesis, University of Southern California, Los Angeles, Cal.

Meinhart, C. D., 1994, Investigation of turbulent boundary layer structure using particle-image velocimetry, Ph.D. thesis, University of Illinois at Urbana-Champaign, Urbana, IL.

Smith, C. R. and Metzler, S. P., 1983, The characteristics of low-speed streaks in the near-wall region of a turbulent boundary layer, *J. Fluid Mech.*, vol. 129, pp. 27-54.

Tomkins, C. D. and Adrian, R. J., 1999, Characteristics of vortex packets in wall turbulence, *Proceedings, First Intl. Symp. on Turbulence and Shear Flow*, Santa Barbara, September.

Wark, C. E. and Nagib, H. M., 1991, Experimental investigation of coherent structures in turbulent boundary layers, *J. Fluid Mech.*, vol. 230, pp. 183-208.

Wark, C. E., Naguib, A. M., and Robinson, S. K., 1991, Scaling of spanwise length scales in a turbulent boundary layer, AIAA Paper No. 91-0235.

Westerweel, J., 1997, Fundamentals of digital particle image velocimetry, *Meas. Sci. Tech.*, vol. 8, pp. 1379-1392.